

Charged Particle Multiplicities at BRAHMS

S.J. Sanders¹ (for the BRAHMS Collaboration),
I.G. Bearden,⁸ D. Beavis,² C. Besliu,¹¹ Y. Blyakhman,⁷ J. Brzychczyk,⁵
B. Budick,⁷ H. Bøggild,⁸ C. Chasman,² C.H. Christensen,⁸
P. Christiansen,⁸ J. Cibor,⁴ R. Debbe,² J.J. Gaardhøje,⁸ K. Grotowski,⁵
K. Hagel,⁹ O. Hansen,⁸ A. Holm,⁸ A.K. Holme,¹² H. Ito,¹ E. Jakobsen,⁸
A. Jipa,¹¹ J.I. Jørdre,¹⁰ F. Jundt,³ C.E. Jørgensen,⁸ T. Keutgen,⁹
E.J. Kim,⁶ T. Kozik,⁵ T.M. Larsen,¹² J.H. Lee,² Y.K. Lee,⁶
G. Løvholden,¹² Z. Majka,⁵ A. Makeev,⁹ B. McBreen,² M. Murray,⁹
J. Natowitz,⁹ B.S. Nielsen,⁸ K. Olchanski,² J. Olness,² D. Ouerdane,⁸
R. Płaneta,⁵ F. Rami,³ D. Röhrich,¹⁰ B.H. Samset,¹² S.J. Sanders,¹
R.A. Sheetz,² Z. Sosin,⁵ P. Staszal,⁸ T.F. Thorsteinsen,^{†10} T.S. Tvetter,¹²
F. Videbæk,² R. Wada,⁹ A. Wieloch⁵ and I.S. Zgura¹¹

¹ University of Kansas, Lawrence, KS 66049, USA

² Brookhaven National Laboratory, Upton, New York 11973, USA

³ Institut de Recherches Subatomiques and Université Louis Pasteur
Strasbourg, France

⁴ Institute of Nuclear Physics, Krakow, Poland

⁵ Jagiellonian University, Krakow, Poland

⁶ Johns Hopkins University, Baltimore, Maryland 21218, USA

⁷ New York University, New York, New York 10003, USA

⁸ Niels Bohr Institute, University of Copenhagen, Copenhagen, Denmark

⁹ Texas A&M University, College Station, Texas 77843, USA

¹⁰ Department of Physics, University of Bergen, Bergen, Norway

¹¹ University of Bucharest, Bucharest, Romania

¹² Department of Physics, University of Oslo, Oslo, Norway

Abstract. Charged particle pseudorapidity densities are presented for the $^{197}\text{Au} + ^{197}\text{Au}$ reaction at $\sqrt{s_{NN}} = 130$ GeV. These densities provide an essential characterization of the underlying reaction mechanisms for ultra-relativistic heavy-ion collisions. This talk details how the global charged particle yields are measured at BRAHMS and presents some preliminary results from the analysis of data taken during the first year of the RHIC experimental program.

Keywords: charged particle densities
PACS: 25.75.Dw

1. Introduction

The number of particles emitted from a heavy-ion collision at RHIC energies provides one of the most basic characterizations of the collision process. On an event-by-event basis, this observable can be related to the centrality of the collision. By analyzing a large number of events, the dependence of the particle multiplicity on pseudorapidity and reaction centrality can be determined. This can further the study how the energy loss by the incident channel leads to particle production. Recent theoretical works have emphasized the importance of determining the particle densities over a range of pseudorapidities and centralities to better understand the relative contributions of “soft” hadronic and “hard” partonic processes and to search for gluon saturation effects [1, 2] in ultra-relativistic heavy-ion collisions.

In this talk, global charged particle measurements using complementary subsystems of the BRAHMS experiment will be described. Differential charged particle distributions in $dN_{ch}/d\eta$ are presented as a function of pseudorapidity η and of reaction centrality for the $^{197}\text{Au} + ^{197}\text{Au}$ reaction at $\sqrt{s_{NN}} = 130$ GeV. The BRAHMS results are compared to other recent results reported by the PHOBOS [3, 4] and PHENIX [5] Collaborations. Comparisons are also made with HIJING model calculations [6].

2. Experimental Arrangement

The BRAHMS detector system (see Fig. 1) consists of two magnetic spectrometers, which allow for the determination of charged particle properties over a wide rapidity and momentum range, and a number of global detectors employed to characterize the general features of the reaction, such as the overall charged particle multiplicity and the flux of spectator neutrons at small angles. The current analysis is based primarily on the global detectors, including the Multiplicity Array, the Beam–Beam Counter Arrays (BB), and the Zero-Degree Calorimeters (ZDC), but also uses data from the front time-projection chamber (TPM1) of the mid-rapidity spectrometer arm.

2.1. Multiplicity array

The multiplicity array provides a measure of charged particle production in the pseudorapidity range of $-3 \leq \eta \leq 3$. The quoted pseudorapidity coverage of the array is greater than the geometric coverage for reactions occurring at the nominal array center because of the extended range where collisions take place along the beam axis. The array consists of an inner barrel of Si strip detectors (SiMA) and an outer barrel of plastic scintillator “tile” detectors (TMA). These detectors are collectively used to establish overall charged particle multiplicities for collisions at BRAHMS.

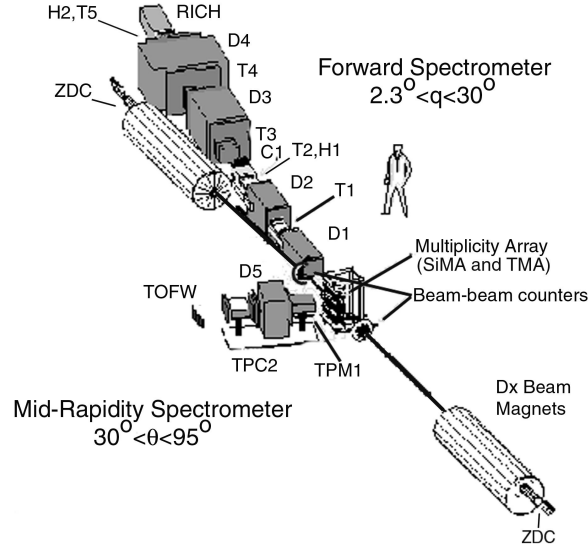


Fig. 1. Schematic of the BRAHMS experiment. Magnetic dipole elements (D1–D5) are sandwiched with tracking chambers of either time projection (T1, T2, TPM1, TPM2) or drift (T3–T5) chamber type. Time-of-flight arrays (H1, H2, TOFW) are used in the particle identification of sub-relativistic particles and Cherenkov counters (C1, RICH) are used for the identification of faster particles. Global charged particle production is determined using the Beam–Beam Counter Arrays, the Si (SiMA) and scintillator tile (TMA) elements of the Multiplicity Array, as well as the TPM1 time projection chamber. The Zero-Degree Calorimeters determine the neutron yields along the beam axis.

The current data were obtained with the Si array configured with 25, $4 \text{ cm} \times 6 \text{ cm} \times 300 \mu\text{m}$ wafers, each segmented into 7 strips with a 0.86 cm pitch. The detectors were located 5.3 cm from the nominal beam axis. The TMA barrel was configured with 38, $12 \text{ cm} \times 12 \text{ cm} \times 0.5 \text{ cm}$ scintillator tiles located 13.9 cm from the nominal beam axis. Light collection from the tiles was done using wavelength shifting optical fibers mounted in a groove machined around the detector perimeter, as described in Ref. [7]. The current arrangement was tested and found to result in a light collection uniformity of better than 5% for particles hitting the central region of a tile. Within 5 mm from a tile edge, however, the response drops off rapidly. The energy calibrations of both the Si and tile detector elements was accomplished by comparing the location of the single-particle peak in the observed energy spectrum to the calculated energy for this peak based on Monte-Carlo simulations of the array response using the GEANT code [8].

Both the Si detectors and scintillator tiles are arranged in six rows of detectors about the beam axis. For the Si strip detectors three rows were populated with six wafers each, covering 42 bins in pseudorapidity, one row was populated with five wafers, and the last two rows were populated with one wafer each. In this arrangement, one “ring” about the beam axis was fully populated. The sparse population of two sides was to accommodate a

clear line-of-sight for the two spectrometer arms and for reasons of cost. The scintillator tile array had four rows fully populated with 8 detectors, each, one row had 4 detectors, and the last row had 2 detectors. Again, the partially populated rows were to accommodate the spectrometer arms. The detectors in each Si and tile row were mounted contiguously, starting with completely populated Si and tile rings at the far end of the array with respect to the forward spectrometer.

For typical collisions at RHIC, the modest segmentation of the multiplicity array results in multiple particles passing through individual detector elements. The number of particles passing through a given element is determined by dividing the total energy observed in that element by the corresponding predicted average energy loss for a single particle as determined through the GEANT simulations. This procedure relies on there being a reasonably well defined average stopping power for the pions, kaons, and protons that dominate the emitted charged particle distributions in a RHIC collision. The particle yields are corrected for secondary scattering contributions using the GEANT simulations of the array response. The HIJING [6] model was used to obtain the primary particle distribution for the GEANT simulation. The secondary scattering corrections are position dependent and range from 20% to 40% for the TMA and from 6% to 25% for the SiMA.

Figure 2 shows how the asymmetric Landau-type shape of the average energy loss spectrum in the Si and tile elements affects the measurement of particle yields in these detectors. The top two panels show the distributions of primary particles expected to hit representative Si and tile elements using central events from the HIJING code [6]. The bottom two panels show histograms of the event-by-event reconstructed number of particles using the procedure of dividing the measured energy by the calculated average energy of a single particle passing through the detector. The average number of particles deduced from each of the spectra is indicated. It is clear that although the event-by-event reconstruction can be strongly distorted because of asymmetric energy-loss distributions for the single particle response, by averaging over a large number of events it is possible to recover the average number of emitted particles.

2.2. Beam-beam arrays

The BB arrays consist of two sets of Cherenkov UV transmitting plastic radiators coupled to photomultiplier tubes. They are positioned around the beam tube on either side of the nominal interaction point with their front faces at a distance of 2.15 m. The left array, located away from the forward spectrometer arm, consists of 8 “large” detectors with 51 mm diameter and 36 “small” detectors with 19 mm diameter, arranged symmetrically around the beam tube. The right array is asymmetric to allow the movement of the forward spectrometer to small angles and consists of 5 large detectors and 30 small detectors. The BB counters have an intrinsic time resolution of 60 ps allowing for the determination of the position of the interaction point with a precision of ≈ 1 cm. The two arrays can be used to determine charged particle multiplicities in the pseudorapidity range $2.5 \leq |\eta| \leq 4.0$ by direct counting of the number of particles hitting each tube. Corrections for secondary scattering events were again based on GEANT simulations, with the correction factors approaching 50% of the measured yield for certain vertex locations. Figure 3 shows a typical

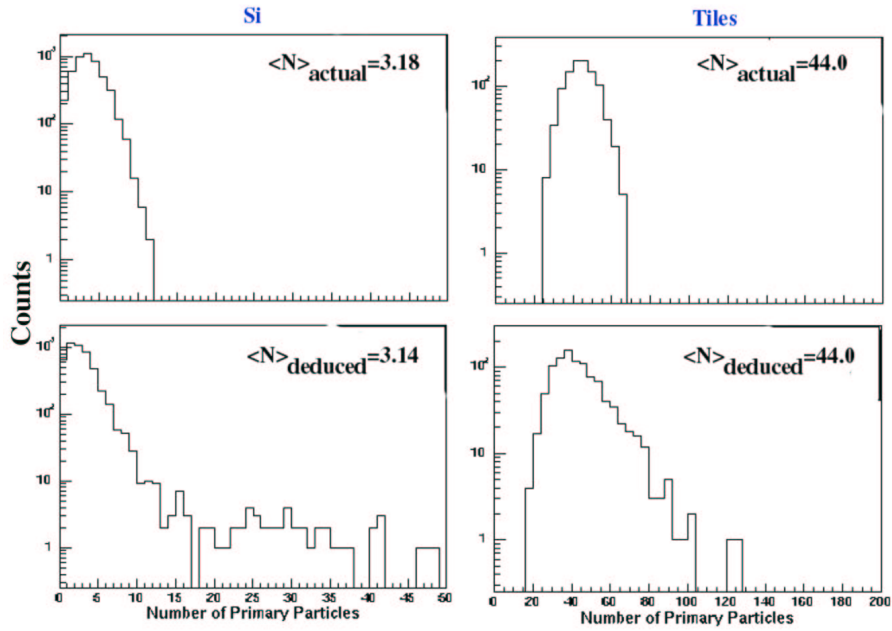


Fig. 2. Reconstruction of the number of emitted particles using Si and tile elements based on simulations. The top two panels show the “actual” particle distributions and the bottom panels show the “recovered” distributions using the procedures outlined in the text.

spectrum obtained with one of the large tubes. The individual hits are clearly resolved for lower hit multiplicities.

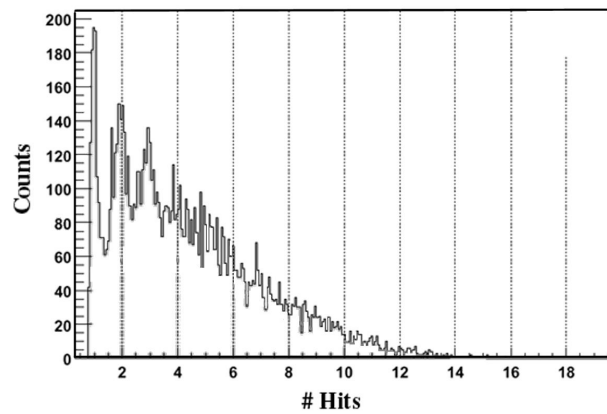


Fig. 3. Typical spectrum obtained with one of the “large” tubes of the beam–beam array

2.3. ZDCs

The two Zero-Degree Calorimeters (ZDCs), positioned on either side of the nominal interaction point at a distance of 18 m, were used to establish a minimum bias trigger for the experiment. The ZDCs measure the energy deposited by spectator neutrons that are emitted to small angles with respect to the beam direction, with $|\theta| < 2$ mrad [9]. Each ZDC consists of alternating layers of tungsten and fiber-ribbon plastic scintillator. The time difference of the two ZDC signals can be used to determine the interaction vertex with a precision of ≈ 3.5 cm.

2.4. Mid-rapidity spectrometer TPC

In addition to the particle densities found using the global detectors, charged particle multiplicities at selected angles can also be obtained using the front time-projection chamber (TPM1) of the mid-rapidity spectrometer arm. In this case, particle multiplicities are deduced by counting tracks in the fiducial volume of the detector that originate from the interaction vertex, with a small correction for background tracks that fulfill these same requirements. Measurements were made at 40° and 90° , respectively.

Although the TPC measurements were obtained at only a few angles, they provide an important cross-check of the analysis procedures. The dominant systematic uncertainties for the TPC measurements arise from a multiplicity-independent background correction and a tracking efficiency correction that depends on the density of position-time “clusters” in the detector. This later density, on average, scales with the overall particle multiplicity. When this density becomes too high, it becomes difficult to reconstruct unique tracks. The tracking efficiency correction is obtained by embedding simulated single tracks into real event data and then determining the reconstruction efficiency. The tracking efficiency ranges from almost unity for low density, peripheral scattering events, to ≈ 0.85 for high-density central events at the 40° setting. By contrast, the dominant systematic uncertainty for the Si and tile detector arrays is the energy calibration obtained for these detectors. Consequently, the dominant TPC and MPA uncertainties are expected to be largely uncorrelated.

3. Multiplicity to Centrality

Minimum biased events are selected by requiring that the ZDC counters establish a vertex within 120 cm of the nominal vertex position and that there be at least one “hit” in the TMA detectors. These two requirements largely remove background contributions from beam-residual gas interactions and from very peripheral collisions involving only electromagnetic processes. The location of the interaction vertex can be determined by using the track reconstruction from TPM1 with a resolution of better than 0.5 cm. For peripheral events where there are insufficient tracks for a vertex determination, the BB array vertex is used. If neither TPM1 or the BB array is able to establish a vertex location, then the ZDC vertex is adopted. For the BB multiplicity analysis, the primary vertex was chosen as that determined

by the BB array, with the TPM1 results used for a consistency check and for calibration purposes.

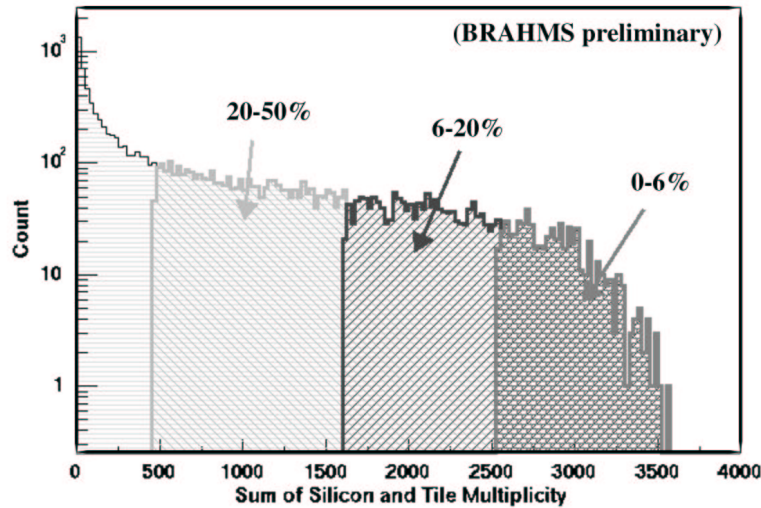


Fig. 4. Sum of the SiMA and TMA multiplicity distributions

Figure 4 shows the multiplicity distribution of charged particles established by the multiplicity array. The independent multiplicity measurements of the SiMA and TMA detectors are summed for this figure. Before summing, the SiMA multiplicity was rescaled to account for the difference in the geometric coverage of the SiMA and TMA arrays. From simulations it is estimated that this summed distribution exhausts $> 97\%$ of the nuclear reaction cross section. With the usual geometrical relation between impact parameter and number of participants, as represented, for example, by Glauber model calculations [10], and further assuming a roughly constant particle production per participant pair, it is expected that a cut on the total multiplicity translates to a cut on collision centrality. The principle centrality cuts used for the current analysis are shown by the different shaded regions in Fig. 4. It is assumed, for example, that the 6% most central events correspond to the 6% of events with the highest particle multiplicity.

Although the actual reaction impact parameter is not a measurable quantity, it is possible to obtain some sense as to how well a multiplicity selection can be related to a centrality selection through model calculations. Figure 5 shows the corresponding multiplicity distribution to that shown in Fig. 4 calculated using the HIJING model. The vertical lines show the corresponding multiplicity cuts for 0–6%, 6–20% and 20–50% on the total multiplicity, respectively. The actual events corresponding to these three centrality ranges are indicated by the shaded regions. It is seen that the achievable experimental cuts on multiplicity do a good job in selecting events in the different centrality ranges.

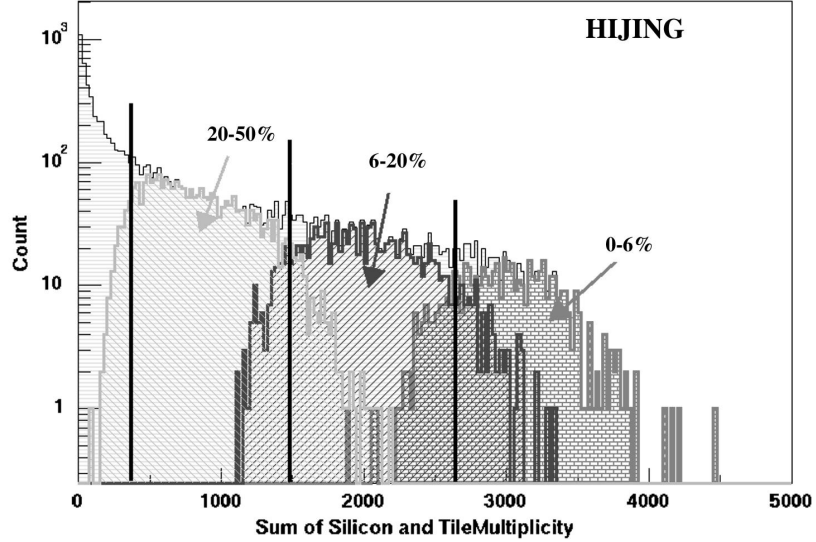


Fig. 5. Calculated charged particle multiplicity distribution for the Si and tile detectors based on the HIJING model. The vertical lines and shaded regions are described in the text.

The centrality selection based on the Si and tile multiplicity could only be calibrated over a range of vertex locations within 45 cm of the nominal center of the multiplicity array. Outside of this range, the corrections for secondary scattering and the extreme angle-of-incidence for particles hitting the Si and tile elements makes a global multiplicity determination doubtful. However, to extend the $dN_{ch}/d\eta$ distributions of the BB array to lower pseudorapidities where they overlap with the Si and tile measurements, it was necessary to use vertex positions ranging out to 120 cm from the nominal array center. For these BB array measurements, the centrality determination was therefore made using the multiplicity data from the BB arrays and the ZDCs. The selection was made on the correlation plot of the ZDCs sum energy vs. BB array multiplicity. These centralities were compared to those obtained with the multiplicity array for events where both measurements were possible and found to be in good agreement.

4. $dN_{ch}/d\eta$ Results

Figure 6 presents the preliminary $dN/d\eta$ distribution measurements for centrality cuts on 0–6%, 6–20% and 20–50% of the total multiplicity distribution. Results are shown for the SiMA, TMA, TPM1 and BB measurements. For the TPM1 data, the up and down triangles correspond to two different analyses of the data using different tracking methods. Uncertainties are only shown for the BB measurements as these uncertainties are still being

assessed for the other detector systems. In general, for all of the data sets, the uncertainties are currently estimated at about a 10% level.

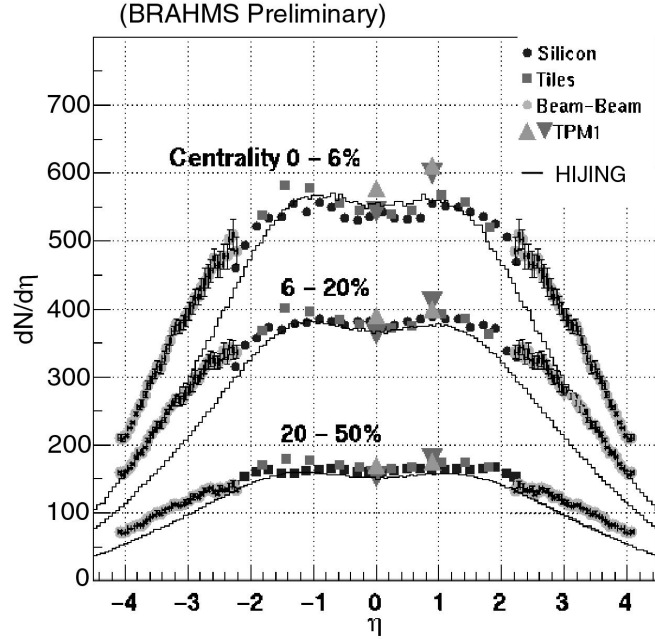


Fig. 6. Charged particle multiplicities as a function of pseudorapidity

The PHOBOS [3] and PHENIX [5] experiments have recently reported values for the charged particle densities at mid-rapidity corresponding to the 6% most central events. PHOBOS obtains $dN_{ch}/d\eta|_{\eta=0} = 555 \pm 12(\text{stat}) \pm 35(\text{syst})$ while PHENIX finds $dN_{ch}/d\eta|_{\eta=0} = 609 \pm 1(\text{stat}) \pm 37(\text{syst})$. For the same centrality range, our result is $dN_{ch}/d\eta|_{\eta=0} = 525 \pm 53(\text{syst})$, where the statistical uncertainty is negligible and a 10% systematic uncertainty is assigned to the results. Within the quoted uncertainties the results for the three experiments are in agreement.

The results of the HIJING model calculations are shown in Fig. 6 by the solid curves. The HIJING calculations are found to reasonably well reproduce the experimental results at mid-rapidity ($\eta = 0$), but to significantly underpredict the width of the distributions for the different centrality cuts.

Figure 7 shows for $\eta = 0$ the charged particle densities normalized to half of the number of participants as a function of the number of participants N_p . The HIJING code was used to obtain the number of participants corresponding to the different centrality cuts. It is seen that the particle production per participant pair has a slight upward slope over the considered centrality interval. The PHENIX results [5] taken at mid-rapidity and preliminary results from the PHOBOS Collaboration [4] are also shown in the figure. The general trend

of these data agree with our observations although, as noted earlier, the overall charged particle densities for PHENIX are somewhat larger than what we observe.

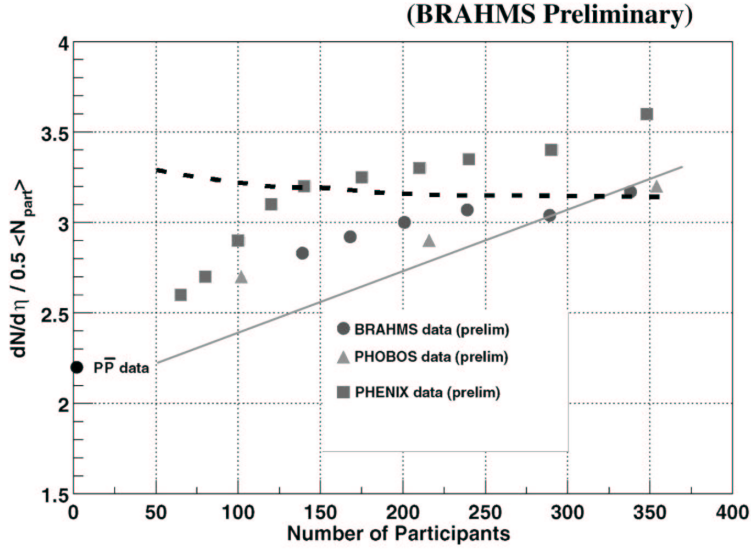


Fig. 7. Distribution of $dN_{ch}/d\eta$ per participant pair at $\eta = 0$. The $p\bar{p}$ data is from Ref. [11]. The HIJING [1] and EKRT [2] model results are indicated by the solid and dashed curves, respectively.

Two model calculations are compared to the data in Fig. 7. The HIJING model [1] contains contributions from both soft and hard processes, where the soft processes are expected to scale with N_p , leading to a constant value of $dN_{ch}/d\eta$ per participant pair, and the hard processes should increase more rapidly. The EKRT model [2] predicts saturation of the gluon density, leading to a relatively flat, but slightly decreasing dependence of $dN_{ch}/d\eta$ per participant pair as a function of the number of participants. The slope of the experimental results appear to be between those of the HIJING and EKRT predictions.

5. Conclusions

In summary, the BRAHMS experiment has measured pseudorapidity densities of charged particles at $\sqrt{s_{NN}} = 130$ GeV over a large range of pseudorapidity as a function of collision centrality using several independent detector systems and methods. The results appear to be in agreement with similar measurements reported by the PHENIX and PHOBOS Collaborations. Although the HIJING model calculations appear to be in good agreement with experiment at mid-rapidity, this model fails to reproduce to width of the observed charged particle distribution as a function of pseudorapidity.

Acknowledgements

This work was supported by the Division of Nuclear Physics of the Office of Science of the U.S. Department of Energy under contracts DE-AC02-98-CH10886, DE-FG03-93-ER40773, DE-FG03-96-ER40981, and DE-FG02-99-ER41121, the Danish Natural Science Research Council, the Research Council of Norway, the Jagiellonian University Grants, the Korea Research Authorities, and the Romanian Ministry of Research (5003/1999, 6077/2000).

Note

† Deceased

References

1. Xin-Nian Wang and Miklos Gyulassy, *Phys. Rev. Lett.* **86** (2001)3496.
2. K.J. Eskola, K. Kajantie and K. Tuominen, preprint hep-ph/0009246.
3. B.B. Back et al., *Phys. Rev. Lett.* **85** (2000) 3100.
4. A. Wuosmaa, Quark Matter 2001 Proceedings (2001).
5. K. Adcox et al., *Phys. Rev. Lett.* **86** (2001) 3500.
6. X. Wang and M. Gyulasy, *Phys. Rev. D* **44** (1991) 3501.
7. S. Aota et al., *Nucl. Instr. Meth.* **A352** (1995) 557.
8. GEANT 3.2.1, CERN program library.
9. C. Adler, A. Denisov, E. Garcia, M. Murray, H. Stroebele and S. White, preprint nucl-ex/0008005.
10. R.J. Glauber and G. Matthiae, *Nucl. Phys.* **B21** (1970) 135.
11. G. Alner et al., *Z. Phys. C* **33** (1986) 1.

